Journal of Photochemistry and Photobiology A: Chemistry 218 (2011) 117–129

Contents lists available at ScienceDirect

Journal of Photochemistry and Photobiology A: Chemistry

journal homepage: www.elsevier.com/locate/jphotochem

Low temperature X-ray diffraction analysis, electronic density distribution and photophysical properties of bidentate *N*,*O*-donor salicylaldehyde Schiff bases and zinc complexes in solid state

Oxana Kotova[a,b,c,*], Konstantin Lyssenko[d], Andrey Rogachev[e], Svetlana Eliseeva[a,b], Ivan Fedyanin[d], Leonid Lepnev[c], Lesley Pandey[f], Anatolii Burlov[g], Alexander Garnovskii[g], Alexey Vitukhnovsky[c], Mark Van der Auweraer[f], Natalia Kuzmina[a]

[a] *Department of Chemistry, Lomonosov Moscow State University, Leninskie Gory 1-3, 119991 Moscow, Russia*
[b] *Department of Materials Sciences, Lomonosov Moscow State University, Leninskie Gory 1-3, 119991 Moscow, Russia*
[c] *Vavilov Luminescence Laboratory, Lebedev Physical Institute of Russian Academy of Sciences, Leninsky Prospect 53, 119991 Moscow, Russia*
[d] *A.N. Nesmeyanov Institute of Organoelement Compounds, Russian Academy of Sciences, GSP-1, 28 Vavilov Street, Moscow 119991, Russia*
[e] *Institut für Anorganische und Angewandte Chemie, Department Chemie, Universität Hamburg, Martin-Luther-King-Platz 6, 20146 Hamburg, Germany*
[f] *Department of Chemistry and Institute for Nanoscale Physics and Chemistry, Katholieke Universiteit Leuven, Celestijnenlaan 200-F, 3001 Heverlee-Leuven, Belgium*
[g] *Institute of Physical and Organic Chemistry of Southern Federal University, 344090 Rostov-on-Don, Russia*

ARTICLE INFO

Article history:
Received 1 August 2010
Received in revised form
13 December 2010
Accepted 14 December 2010
Available online 23 December 2010

Keywords:
Synthesis
High resolution XRD analysis
Charge density analysis
Theoretical calculation
Luminescence

ABSTRACT

Zinc complexes (ZnL_2) with bidentate *N*,*O*-donor Schiff bases (HL = HSH1, HSH2, HSH3) derivatives of salicylaldehyde and *para*-substituted anilines were synthesized and fully characterized. The crystallographic parameters of HSH2 and ZnL_2 were refined. Low temperature X-ray diffraction analysis including topological analysis of electron density function for crystals of ZnL_2 reveals that the geometrical parameters of all investigated compounds as well as the charges in chelate rings of complexes remain almost unchanged upon variation of the substituents (R) in *para*-position of the aniline fragment, going from $-CH_3$ (HSH1) to $-N(CH_3)_2$ (HSH2) and $-OCH_3$ (HSH3). Zinc complexes are thermally stable up to ~190 °C as shown by thermogravimetric analysis under nitrogen atmosphere. The photoluminescent (PL) properties of HL and ZnL_2 were investigated in the solid state while its absorption spectra were measured in methanol. The theoretical calculation of the investigated compounds confirmed firstly the existence of *enol-imine* and *keto-enamine* tautomeric forms; and secondly the influence of the introduction of R on the PL properties of the compounds. The study of excited state dynamics of ZnL_2 in the solid state shows bi-exponential fluorescence decays and relatively high PL quantum yield, making them potentially adequate for being used as manifold optical materials. The interpretation of photophysical properties are substantiated by DFT and TD-DFT theoretical calculations of the Schiff bases and zinc complex species.

1. Introduction

In the past decades, significant progress has been achieved in understanding the chemistry of transition metals complexes with Schiff base ligands composed of salicylaldehyde [1].

Besides showing excellent catalytic activity [2] and magnetic properties [3], these metallic complexes can be used as well in medicine as anti-cancer drugs [4], sensors [5] and in different optical materials [6,7]. In view of the latter application zinc complexes attract a special attention since along with high light emitting efficiency and possibility of easy tuning the luminescent properties by variation the nature of substituents in organic ligands, they are inexpensive, nontoxic, possess high thermal stability, volatility and solubility. Moreover, zinc complexes with Schiff bases are prospective precursors for controlled organization of nanoscale patterns and wires [8], optoelectronic technology thanks to their non-linear optical properties [9], fluorescent sensors for detection of chemical explosives [10] and electroluminescent (EL) layers in organic light emitting diodes (OLEDs) [11,12].

Within the sight of being applied as EL materials for OLEDs, different classes of complexes have been explored by our research groups [13,14]. According to literature [11,12] and our investigations [14,15] zinc complexes with bi- and tetra-dentate (*N*,*O*-donor atoms) Schiff bases can be suggested and some of them have been already used to build up OLED systems. In order to find out new EL materials among these complexes one should not only know

* Corresponding author at: Department of Chemistry, Department of Materials Sciences, Lomonosov Moscow State University, Leninskie Gory 1-3, 119991 Moscow, Russia. Tel.: +7 495 939 38 36; fax: +7 495 939 09 98.
E-mail address: kotova@inorg.chem.msu.ru (O. Kotova).

1010-6030/$ – see front matter © 2010 Elsevier B.V. All rights reserved.
doi:10.1016/j.jphotochem.2010.12.011

Table 1
Crystal data and some details of data collection and structures refinement for HSH2 and $Zn(SH1)_2$, $Zn(SH2)_2$, $Zn(SH3)_2$ compounds.

Compound	HSH2	$Zn(SH1)_2$	$Zn(SH2)_2$	$Zn(SH3)_2$
Formula unit	$C_{15}H_{16}N_2O$	$C_{28}H_{24}N_2O_2Zn$	$C_{30}H_{30}N_4O_2Zn$	$C_{28}H_{24}N_2O_4Zn$
Molecular weight	240.30	485.86	543.95	517.86
Temp [K]	100	100	100	100
Crystal system	Orthorhombic	Monoclinic	Triclinic	Triclinic
Space group	*Pbca*	*C2/c*	*P*-1	*P*-1
Z (Z')	8 (1)	4 (0.5)	4 (2)	2 (1)
a (Å)	11.175(1)	22.126(2)	10.1357(4)	8.9833(2)
b (Å)	7.9742(8)	8.495(2)	16.4960(7)	11.3085(2)
c (Å)	27.409(3)	11.907(2)	17.3308(7)	12.0086(2)
α (°)	90.00	90.00	115.1170(10)	84.2710(10)
β (°)	90.00	95.404(4)	95.9150(10)	87.4980(10)
γ (°)	90.00	90.00	98.3080(10)	71.8090(10)
V (Å^3)	2442.5(4)	2228.1(6)	2552.08(18)	1153.07(4)
ρ_{calc} (g cm^{-3})	1.307	1.448	1.416	1.492
μ (cm^{-1})	0.83	11.31	9.98	11.04
F(000)	1024	1008	1136	536
$2\theta_{max}$ (°)	58	100	60	100
Reflections measured (R_{int})	17091 (0.0800)	132187 (0.0304)	33528 (0.0313)	139845 (0.0297)
Independent reflections	3538	11688	14850	23867
Observed reflections [$I > 2\sigma(I)$]	2244	10346	11675	20527
Number of parameters	165	199	675	412
Final $R(F_{hkl})$: R_1	0.0482	0.0223	0.0348	0.0246
wR_2	0.1218	0.0700	0.0809	0.0727
GOF on F^2	1.019	1.041	1.026	1.018
$\Delta\rho_{max}/\Delta\rho_{min}$ (eÅ^{-3})	0.295/−0.251	0.577/−0.317	0.432/−0.543	0.711/−0.458

about the influence of different substituents on their photophysical properties, thermal stability, volatility and solubility but also about the electronic structure of the complexes. Indeed, information about the valence orbitals (highest occupied molecular orbital, HOMO; lowest unoccupied molecular orbital, LUMO) is essential to get the optimal structure leading to the most efficient OLED [12,16]. In our previous work [15(a)] both experimental and theoretical data have been utilized to discuss the influence of substituents such as an extending of π-conjugation or an increasing of donor character on the properties of tetradentate Schiff base derivatives of salicylaldehyde and their zinc complexes.

Recently, EL materials based on zinc complexes with bidentate *N,O*-donor Schiff bases derivatives of salicylaldehyde and *para*-substituted anilines (R = –CH_3 (HSH1), –$N(CH_3)_2$ (HSH2), –OCH_3 (HSH3)) have been shown to demonstrate sufficient electron transport ability and were successfully incorporated into OLEDs [12]. Herein we focused our study on the peculiarities of molecular geometry and investigated how structural changes can influence the overall photophysical properties of such compounds in solid state, including time-correlated single photon counting measurements and absolute quantum yields determination. To achieve further understanding on the relation between structure and optical properties, a comprehensive analysis of Schiff base and zinc complexes crystals was carried out by measuring low-temperature X-ray diffraction as well as performing both theoretical and experimental electron density distribution analyses.

2. Experimental

2.1. Synthesis of the ligands (HL) and zinc complexes (ZnL_2)

The full synthesis methodology and characterization of Schiff bases and zinc complexes are reported in the Supporting Information.

2.2. X-ray crystallography

X-ray diffraction experiments were carried out with a Bruker SMART APEX II CCD area detector, using graphite monochromated Mo-Kα radiation (λ = 0.71073 Å) at 100 K. Reflection intensities were integrated using SAINT software and absorption correction was applied semi-empirically using SADABS program [17]. The structures were solved by direct method and refined by the full-matrix least-squares against F^2 in anisotropic approximation for non-hydrogen atoms. The hydrogen atoms were located from the Fourier density synthesis and refined in anisotropic approximation for HSH2, $Zn(SH1)_2$ and $Zn(SH3)_2$ and in "riding model" for $Zn(SH2)_2$. Crystal data and structure refinement parameters for HSH2, ZnL_2 are given in Table 1. All calculations were performed using the SHELXTL software [18].

CCDC-753778 (for HSH2), −732184 (for $Zn(SH1)_2$), −732185 (for $Zn(SH2)_2$), −732186 (for $Zn(SH3)_2$) contain the supplementary crystallographic data for this paper. These data can be obtained free of charge from The Cambridge Crystallographic Data Centre via www.ccdc.cam.ac.uk/data_request.cif.

2.3. High resolution X-ray diffraction analysis of electronic density distribution (EDD)

The multipole refinement of $Zn(SH1)_2$ and $Zn(SH3)_2$ was carried out within the Hansen–Coppens formalism [19] using XD program package [20] with the core and valence electron density derived from wave functions fitted to a relativistic Dirac–Fock solution. Before the refinement the C–H bond distances were normalised to ideal values 1.08 Å according to neutron diffraction data. The level of multipole expansion was hexadecapole for metal atom and octupole for all other non-hydrogen atoms. The refinement was carried out against F and converged to R = 0.0144, Rw = 0.0183 and GOF = 0.7904 (for 11108 merged reflections with $I > 3\sigma(I)$) for $Zn(SH1)_2$, to R = 0.0156, Rw = 0.0166 and GOF = 0.9024 (for 18912 merged reflections with $I > 3\sigma(I)$) for $Zn(SH3)_2$. All bonded pairs of atoms satisfy the Hirshfeld rigid-bond criteria (the maximum difference of the mean square displacement amplitude was observed for Zn–O bond and was 11×10^{-4} Å^2) [21]. The potential energy density $\nu(\mathbf{r})$ was evaluated through the Kirzhnits approximation for the kinetic energy density function $g(\mathbf{r})$. Accordingly, the $g(\mathbf{r})$ function is described as $(3/10)(3\pi^2)^{2/3}[\rho(\mathbf{r})]^{5/3} + (1/72)|\nabla\rho(\mathbf{r})|^2/\rho(\mathbf{r}) + 1/6\nabla^2\rho(\mathbf{r})$, what in

conjunction with the virial theorem ($2g(\mathbf{r}) + v(\mathbf{r}) = 1/4\nabla^2\rho(\mathbf{r})$) [22] leads to the expression for $v(\mathbf{r})$ and makes possible to estimate the electron energy density $h_e(\mathbf{r})$. The total electron density function was positive everywhere and the maxima of residual electron density located in the vicinity of nuclei were not more than 0.35 eÅ^{-3}. Analysis of topology of the $\rho(\mathbf{r})$ function was carried out using the WinXPRO program package [23].

2.4. Materials and physical measurements

Elemental analysis (C, H, N) was performed by the Microanalytical Service of the Center for Drug Chemistry (Moscow, Russia). IR spectra were recorded in the range 4000–600 cm^{-1} using a Perkin-Elmer Spectrum One spectrometer equipped with a universal attenuated total reflection sampler. ^{1}H NMR spectra were recorded on an Avance-400 (Bruker, 400 MHz) spectrometer. Thermogravimetric analysis was performed on a Q-1500 thermal analyzer in nitrogen atmosphere at a heating rate of 5 °C min^{-1}. UV–vis absorption spectra of Schiff bases and zinc complexes in methanol solutions at a concentration of 10^{-5} M were recorded with Lambda 35 spectrophotometer (Perkin Elmer) with 1 cm quartz Suprasil® cells. The same instrument with a slightly different setup was used to get reflectance spectra of the solid state samples. Both of these measurements were performed at 298 K.

Luminescence spectra of the samples in solid state were measured on a multi-channel spectrometer S2000 (Ocean Optics) utilizing a nitrogen laser LGI-21 (λ_{ex} = 337 nm) as an excitation source at 298 and 77 K. All emission spectra were corrected for the instrumental functions. Quantum yield of HSH1 in solid state was determined with a Fluorolog FL3-22 spectrofluorimeter at 298 K, under excitation at 337 nm according to an absolute method by using home-modified integration sphere [24]. This sample was measured several times under slightly different experimental conditions. The quantum yields of HSH2, HSH3 and ZnL_2 were calculated relative to the value of absolute quantum yield determined for HSH1 using the following equation [25]:

$$Q_x = Q_r \left(\frac{1 - R_r}{1 - R_x}\right)\left(\frac{\phi_x}{\phi_r}\right),$$

where Q – the quantum yield, R – the amount of reflected excitation radiation, ϕ – the integrated area of the corrected luminescence spectra, subscript x stands for the sample and r for the standard. The estimated accuracy for quantum yield is ±10–20%.

The time-resolved properties and excited state dynamics of our compounds in solid state were studied using the time-correlated single photon counting (TCSPC) technique. The TCSPC setup consists of 2 diode lasers at 809 nm which pump a Millenia XS CW-laser (Spectra Physics), generating light at 532 nm after frequency doubling. This light in turn pumps a Tsunami Ti:sapphire (Spectra Physics), resulting in pulsed laser light, which is tunable between 760 and 1100 nm, at a frequency of 82 MHz. The pulse frequency is reduced to 8.2 MHz using a Pulse Selector 3980 (Spectra Physics) after which the laser light is either doubled or tripled with a flexible harmonic generator (GWU-FHG from GWU Lasertechnik) generating excitation light, tunable between 240 and 500 nm. Emission from the sample was detected at magic angle (54.7°) with a cooled R3809 MCP-PMT from Hamamatsu after passing through a monochromator and being processed using a SPC 430 (Becker & Hickl GmbH) computer card. The instrument response function (IRF) was recorded using a LUDOX scattering solution and its FWMH amounted to ~20 ps.

The fluorescence decay curves were analyzed by being fitted to a convolution of the IRF with a decay function for a δ-pulse using a TRFA Global Analysis Program based on a Marquard–Levenberg minimalisation algorithm and Gaussian-weighted nonlinear least-squares fitting. Decay curves were fitted to a multi-exponential decay function. The quality of each fit was assessed by the random distribution of the residuals, their autocorrelation function and the value of the reduced chi-square parameter (χ^2), which was around 1.1.

2.5. Theoretical calculations

Theoretical calculations were done using PC GAMESS version of GAMESS-US program package [26] for quantum chemistry modeling. Visualization of equilibrium geometries as well as of molecular orbitals was performed using ChemCraft program package [27]. Geometry optimizations of Schiff bases and zinc complexes were calculated at DFT level. The computation of organic molecules HSH1, HSH2 and HSH3 were done using the exchange-correlation parameter-free hybrid functional of Perdew–Burke–Ernzerhof (PBE0) [28]. All atoms of the Schiff bases were described using triple-zeta quality basis sets 6-311G(d,p). Calculations of the zinc complexes were performed using the widely known hybrid functional of Becke–Lee–Yang–Parr (B3LYP) [29]. The zinc atom was described using the Hay and Wadt effective core potential (ECP) along with the LANL2DZ basis set while all the other atoms of organic ligands were described as previously using the 6-311G(d,p) basis sets. The geometry optimization for all the complexes was calculated in a C_2 symmetry point group while for the organic molecules no symmetry restrains were applied. The norm of the gradient for the geometry optimization was accepted to be equal to 10^{-5}. The true minima on the potential energy surfaces were controlled via calculation of the Hessian matrix followed by calculation of the harmonic frequencies. The lack of imaginary frequencies indicated that the true minimum was achieved. The vertical transitions were calculated for the molecules in their ground state optimized geometries using the time-dependent density functional theory (TDDFT) and the same combinations of functional and basis sets as described above. The wavelength corresponding to the vertical $S_0 \rightarrow S_i$ transition and the oscillator strengths of each transition were calculated in order to compare with experimental data and to understand the nature of the main excited states. It should be noted that the wavefunction Ψ_I is:

$$\Psi_I = \sum_{i \in occ} \sum_{j \in virt} C_{ij}^I \Phi_{i \rightarrow j}$$

where $\phi_{i \rightarrow j}$ – the determinant representing an excitation from the occupied molecular orbital (MO) φ_i towards the virtual MO ψ_j; C_{ij}^I – the weight of the determinant in the wavefunction Ψ_I. Thus, the nature of the states analysis was supported by the values of the C_{ij}^I coefficients in the TD-DFT wavefunction and the shapes of the DFT MOs. It was assumed that the DFT MOs were suitable for a good description of the electronic structure of molecules as the Hartree-Fock or extended Hückel MOs methods [30,31]. The peaks were calculated instead of bands since vibrational motion of atoms and solute-solvent dynamical interactions were not taken into account. In order to cover the range of wavelengths above 170 nm the thirty lowest singlet excited states were computed for all systems under consideration.

3. Results and discussion

3.1. Characterization

The composition of investigated bidentate Schiff bases (HL = HSH1, HSH2, HSH3) was ascertained by elemental analysis, IR and ^{1}H NMR spectroscopy. The IR spectra of HL display the typical ν(C=N) modes around 1620 cm^{-1}, δ(O–H) (1400–1000 cm^{-1}), the vibration of the aromatic ring and also ν(C–H) + ν(N–H) at 3300–2500 cm^{-1} range. IR spectroscopy data together with ^{1}H

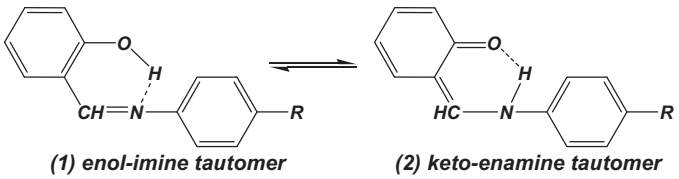

Fig. 1. Proton transfer in Schiff bases.

NMR indicate the possibility of proton transfer in Schiff bases resulted in the existence of tautomeric forms (Fig. 1) [32,33].

The composition of ZnL_2 was confirmed by elemental analysis, IR and NMR spectroscopy. The IR spectra show the characteristic vibration ν(C–H) in the region 3080–2800 cm^{-1}, ν(C=N) 1612–1610 cm^{-1}, ν(C–O) 1190–1030 cm^{-1} and aromatic ring. It was shown that NMR spectra of zinc complexes do not have broad singlet signals at δ ~13.73–13.40 ppm that confirms the absence of initial Schiff base impurities.

3.2. Molecular structures and electron density distribution

According to previous X-ray diffraction analysis there are two possible polymorphic forms of HSH2, namely "red" and "yellow" ones [34,35]. In the molecules of "red" HSH2 the substituent $-N(CH_3)_2$ located coplanar with aniline ring while in "yellow" it is twisted out from this plane to ~7.1°.

Therefore, in the crystal structure of the "red" form HSH2 molecules are located closer to each other with higher interaction energy than in the "yellow" one. Both of these modifications correspond to *enol-imine* tautomer while possessing different photoluminescent properties due to the slight peculiarities of the crystal structures [35]. X-ray diffraction analysis (Fig. 2) shows that HSH2 obtained from benzene solution crystallizes as the "red" form. The main bond lengths and angles in HSH2 at 100 K and room temperature are close to each other [34]. In particular, geometrical parameters of intramolecular O–H···N hydrogen bond are identical; the O(1)···N(1) distance is 2.567(2) and 2.564(4) Å, respectively. The molecule in the crystal is almost planar with the value of the dihedral angle between two aromatic rings being equal to 8.9°. The nitrogen atom of the $-N(CH_3)_2$ group is planar (the sum of CNC bond angles is 360°). The HSH2 molecule in the crystal participates in the formation of weak stacking interaction (C(8)···C(8) 3.540(3) Å) and a number of C–H···π contacts. The molecules of HSH1 are planar and packed along the shortest crystallographic direction *c* [36]. The crystallographic parameters of HSH3 are unknown.

In this work we examined ZnL_2 in order to elucidate the influence of the *para*-substituent in the aniline fragment of the ligand on the peculiarities of the molecular geometry and charge density distribution of the zinc complexes. Since, the structural data of ZnL_2 are available at room temperature [37–39] we investigated their characteristics at low temperature (100 K) (Fig. 3). All the studied zinc complexes crystallize without solvent molecules. In the crystal structure of $Zn(SH1)_2$, molecules are characterized by C_2 symmetry (C_2 axis passes through the Zn(1) atom), while in the structures of $Zn(SH2)_2$ and $Zn(SH3)_2$, it has C_1 symmetry (Fig. 3). The crystal structure of $Zn(SH2)_2$ consists of two independent molecules (Fig. 3(b)). For all complexes, the coordination sphere of Zn(1) atom was found to be formed by two bidentate ligands. The coordination polyhedron of the zinc atom corresponds to a distorted tetrahedron with a dihedral angle between the ZnON planes varying in the range of 79.8–93.8°. The conformation of 6-membered metallocycles can be described as sofa with the deviation of Zn(1) atom from the plane of the NC_3O ones. It should be noted that this cycle is very flexible, and the value of Zn(1) atom deviation (d_{Zn}) in the studied complexes vary from 0.7 Å in $Zn(SH1)_2$ up to 0.05 Å in one of the independent molecules of $Zn(SH2)_2$.

One could expect that the variation of the substituents R ($-CH_3$, $-N(CH_3)_2$ and $-OCH_3$), having different inductive and mesomeric effects, leads to significant redistribution of bond lengths in metallocycles (see Fig. 4). However, analysis of the ZnL_2 geometry (Table 2; Fig. 4) shows that it remains practically the same upon the change of R.

The same is true for the conformation of the ligand. This can be illustrated by analyzing the bond lengths distribution in two independent molecules of $Zn(SH2)_2$. Indeed, the twist angle (ϕ) of the benzene ring in respect to the chelate OC_3N moiety in two independent molecules is 2.6–40.2°, while the C–N bond lengths for the dimethylaniline substituent are almost identical (1.432(2) to 1.434(2) Å) (*e*, Table 2). The increase of d_{Zn} causes only slight variation of Zn–O and Zn–N bonds, while the corresponding bonds in the chelate cycles remain the same. Moreover, the variation of coordination bond strengths (for example, the Zn–O (1.923(1)–1.909(1) Å) distance in $Zn(SH2)_2$) does not have any significant influence on the distribution of the bond lengths in the ligand moiety (Table 2).

The only parameter varying significantly is the length of $C–N(CH_3)_2$ bond in $Zn(SH2)_2$. It increases from 1.375(2) to 1.395(2) Å accompanied by the pyramidalization of nitrogen atom with the sum of CNC bond angles changing from 359.9° to 349.1°. The shortest $C–N(CH_3)_2$ bond length in $Zn(SH2)_2$ is close to that in noncoordinated ligand (HSH2).

The comparison of bond lengths for the HSH2 molecule and its complex clearly shows that the bonding with zinc atom mostly affects C–O and C–N bonds (entries *a* and *e* in Table 2), while the variation of all others is within 0.02 Å. In turn, the elongation of C–N bond (entry *e*) in complex compared to the HSH2 molecule indicates the decrease in conjugation between imine nitrogen atom and its aromatic substituent. Thus, we can conclude that the formation

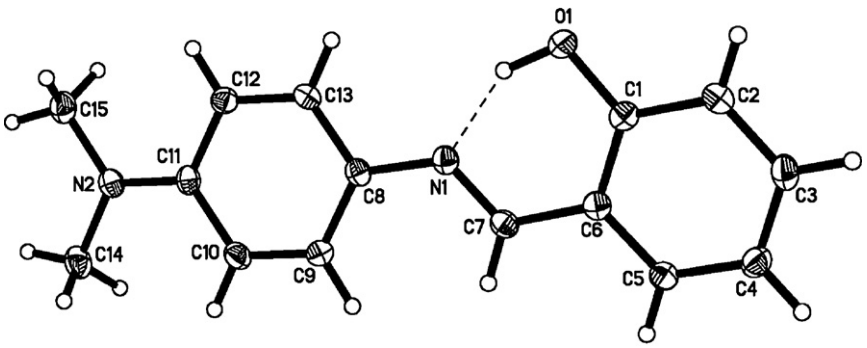

Fig. 2. Molecular structure of HSH2 with thermal ellipsoids set at the 50% probability.

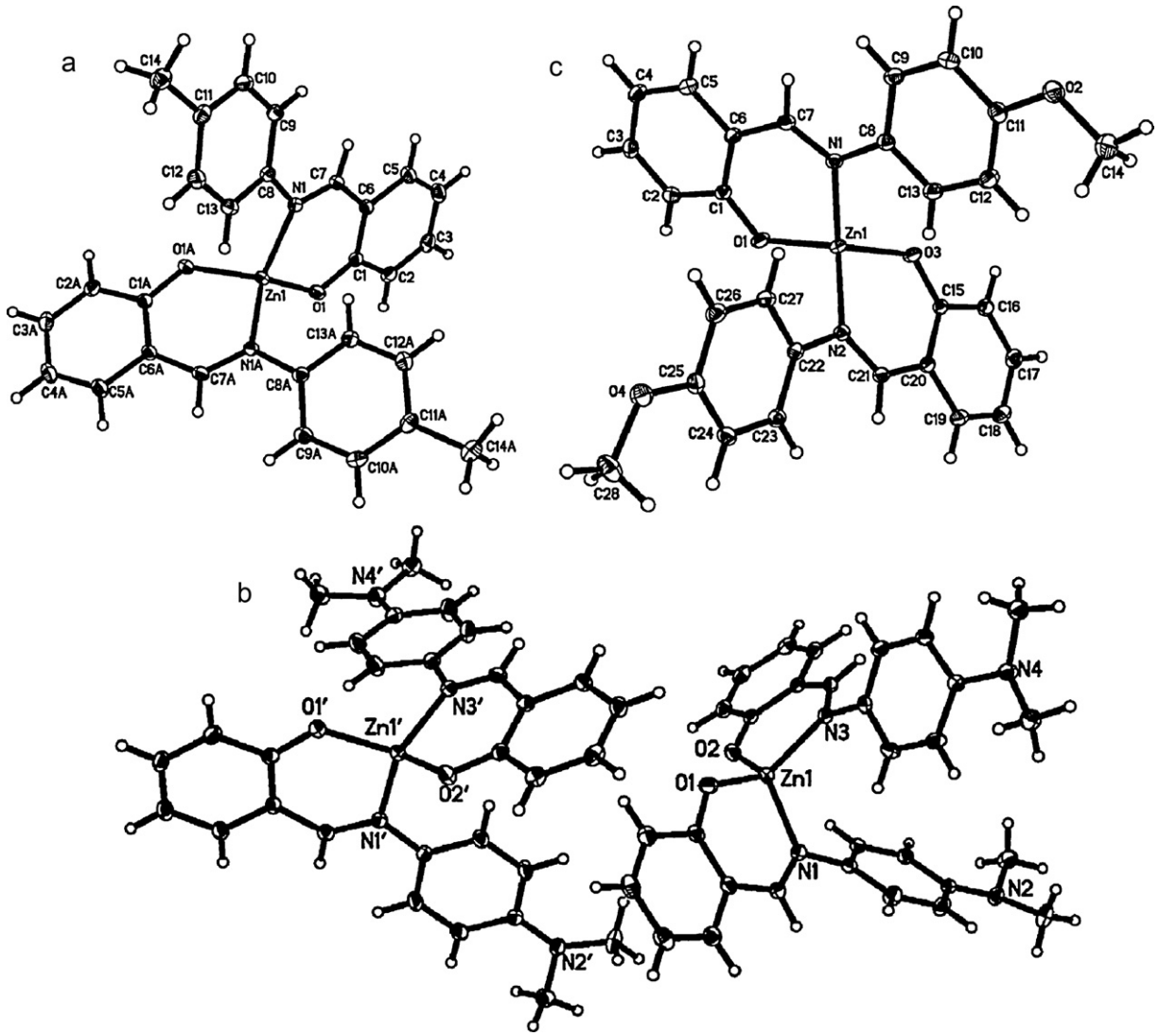

Fig. 3. Molecular structures of (a) $Zn(SH1)_2$, (b) $Zn(SH2)_2$, (c) $Zn(SH3)_2$ with thermal ellipsoids set at the 50% probability.

Table 2
Selected bond lengths and angles of HSH2, $Zn(SH1)_2$, $Zn(SH2)_2$ and $Zn(SH3)_2$; the letters *a*–*f* correspond to distances depicted in Fig. 4.

Parameter	$Zn(SH1)_2$	$Zn(SH2)_2$	$Zn(SH3)_2$	HSH2
Zn–O (Å)	1.9279(4)	1.909(1)–1.922(1) 1.917	1.9162(3)–1.9269(3) 1.921	–
Zn–N (Å)	2.0164(4)	2.009(1)–2.197(1) 2.014	2.0078(3)–2.0122(3) 2.010	–
d_{Zn} (Å)[a]	0.14	0.049–0.22	0.076–0.28	–
a (Å)	1.3127(5)	1.307(2)–1.312(2) 1.309	1.3047(5)–1.3123(5) 1.302	1.353(2)
b (Å)	1.4374(6)	1.426(2)–1.429(2) 1.428	1.4307(6)–1.4302(5) 1.430	1.411(2)
c (Å)	1.4476(6)	1.438(2)–1.444(2) 1.442	1.4426(6)–1.4433(5) 1.443	1.455(2)
d (Å)	1.3069(5)	1.299(2)-1.301(2) 1.300	1.3034(5)–1.3017(5) 1.302	1.287(2)
e (Å)	1.4331(5)	1.431(2)–1.433(2) 1.433(2)	1.4270(5)–1.4295(5) 1.428	1.409(1)
f (Å)	1.5097(6)	1.375(2)–1.395(2)	1.3661(6)–1.3675(5) 1.366	1.369(2)
ϕ (°)	14.1	2.6–40.2	9.1–17.6	4.8
ZnON/ZnON (°)	79.8	75.8–93.8	80.2	–

[a] Out of the metallocycle plane deviation for zinc atom.

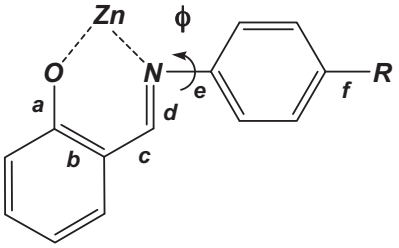

Fig. 4. Schematic representation of half of the ZnL_2 molecules with geometrical definitions.

of zinc complex significantly reduces the influence of substituents in *para*-position of organic ligands HL.

The intermolecular contacts in all zinc complexes studied correspond to weak van der Waals intermolecular interactions. The only exception is $Zn(SH3)_2$, where the stacking interaction was observed (Fig. S1, Supporting Information). However the overlapping occurs only between the symmetry equivalent species (the shortest C···C distance is 3.353(2) Å).

To get more insight into chemical bonding in the zinc complexes we have performed the charge density analysis for two of the above complexes, $Zn(SH1)_2$ and $Zn(SH3)_2$ (Tables S1–S5, Supporting Information). Unfortunately, the low reflection intensity of the $Zn(SH2)_2$ precluded the high resolution X-ray diffraction analysis. The analytical form of the electron density function has been obtained using the multipole model (see Section 2).

The experimental charge density distribution was analyzed in terms of Bader's "Atoms in Molecules" (AIM) theory [22]. The latter not only gives the direct information on the presence and type of chemical bonds, but even provides a possibility to estimate their energy [40]. During last years varieties of investigations [41] demonstrated that the application of the topological analysis of the electron density distribution function ($\rho(\mathbf{r})$), derived from experimental data and/or from theoretical calculations, in conjunction with Espinosa's correlation scheme [42] allows estimating the interaction energy (E_{cont}) with sufficient accuracy. This approach is valid for the qualitative and semi-quantitative description of weak closed-shell interactions as well as the stronger intermediate type of interactions like short O–H···O interactions and coordination bonds, such as Gd–OH_2 and Au–P [43].

The deformation electron density (DED) distribution for both zinc complexes is similar. Its maxima are observed in the vicinity of the zinc, oxygen and nitrogen atoms and in the interatomic area of chemical bonds (Fig. 5). The cross-like accumulation maximum around the zinc atom can be associated with 3d-orbitals, while the maxima around oxygen and nitrogen correspond to their electron lone pairs. The slight variation of the DED distribution around the Zn(1) atom in two complexes is a clear consequence of 5-membered ring puckering. Despite of this variation, the Zn–O and Zn–N interactions in both complexes correspond to "peak to peak" type.

The topology of $\rho(\mathbf{r})$ function in two complexes is slightly different. The critical point (CP) search revealed the presence of CP(3,−1) not only for all of the observed Zn–X, C–C, C–O, C–N, and C–H bonds but also for some shortened intramolecular contacts, such as H···H and, more surprisingly for Zn···H ones. Indeed, in the case of $Zn(SH3)_2$ complex, in which the twist angle ϕ is significantly lower than that in $Zn(SH1)_2$, distances between two protons, namely H(7′)···H(13′) and H(7)···H(9), are as low as 1.87 and 1.89 Å, while in the $Zn(SH1)_2$ this value increases up to 1.97 Å. Although in both structures these contacts are shorter than the sum of the corresponding Van der Waals radii, it corresponds to a bonding interaction only for the $Zn(SH3)_2$. Such dependence of the molecular graph on the twist angle value is well-known, and was analyzed in detail for the biphenyl molecule [44]. In turn, the Zn···H interaction is also observed only for one shortened contact Zn(1)···H(9′) of 2.48 Å in $Zn(SH3)_2$ *vs.* 2.59–2.68 Å in $Zn(SH1)_2$. Based on this geometrical criteria, we may propose that such contacts are also absent in the $Zn(SH2)_2$ complex, where the corresponding intramolecular Zn···H contact is longer than 2.59 Å. In summary, we can conclude that in the $Zn(SH3)_2$ complex the coordination number of zinc atom according to topological analysis is five (Fig. 6) while in both other complexes it is four.

The above Zn···H and H···H interactions in $Zn(SH3)_2$ lead to the presence of three additional CP(3,+1) in comparison with $Zn(SH1)_2$. As one can see, the distance between CP(3,+1) and (3,−1) for these intramolecular contacts is different. For the cycle formed via the H(7)···H(9) binding it is only 0.08 Å, while in the case of the Zn(1)···H(9′) interactions it is slightly longer and is equal to 0.25 Å. Small separation of CP (3,−1) and (3,+1) agrees with the instability of this interaction and its conformational dependence.

According to topological parameters at CP (3,−1) the interactions in complexes can be separated into three groups: (1) shared interactions – all covalent C–C, C–H, C–O and C–N bonds; (2) intermediate interactions – Zn–O and Zn–N bonds; and (3) closed shell ones – intramolecular H···H and Zn···H contacts.

Topological parameters at the CP (3,−1) (Table 3) confirm above conclusions based on geometrical data (Tables 1 and 2). The values of $\rho(\mathbf{r})$ and $\nabla^2\rho(\mathbf{r})$ in CP (3,−1) for bonds of chelate cycle slightly varies and the maximum does not exceed 0.1 eÅ^{-3} and 1.5 eÅ^{-5}, respectively (Table 3). The values of ellipticity (ε), which indicates the contribution of π component, clearly show that zinc atom does not participate in delocalization of π-density and the later is predominantly localized at C–C and C–H bonds.

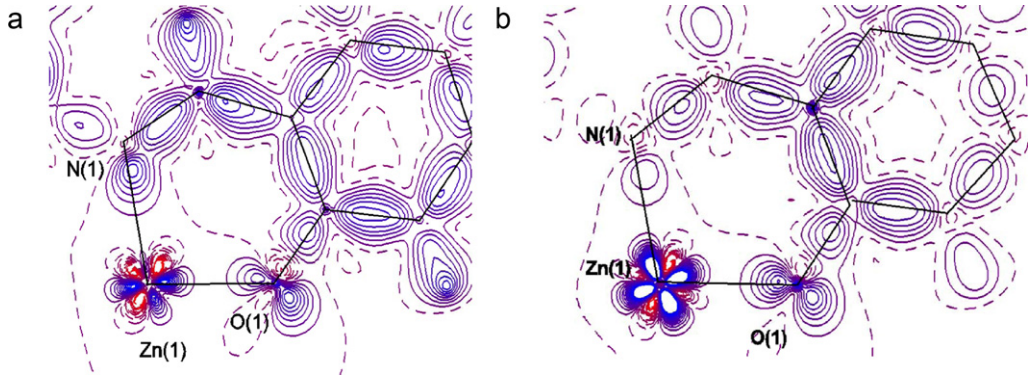

Fig. 5. Section of DED in the plane of Zn(1), O(1) and N(1) atoms in (a) $Zn(SH1)_2$ and (b) $Zn(SH3)_2$. The DED contours are drawn with 0.1 eÅ^{-3} steps (dashed lines correspond to negative values).

Table 3
Topological parameters in $Zn(SH1)_2$ and $Zn(SH3)_2$.

Bond	$Zn(SH1)_2$			$Zn(SH3)_2$		
	$\rho(\mathbf{r})$, eÅ^{-3}	$\nabla^2\rho(\mathbf{r})$, eÅ^{-5}	ε	$\rho(\mathbf{r})$, eÅ^{-3}	$\nabla^2\rho(\mathbf{r})$, eÅ^{-5}	ε
O(1)–C(1)	2.34	−20.2	0.12	2.39	−22.7	0.06
N(1)–C(7)	2.48	−27.5	0.18	2.59	−27.1	0.18
N(1)–C(8)	1.90	−10.7	0.15	1.94	−11.5	0.12
C(1)–C(2)	1.97	−14.9	0.19	2.04	−16.5	0.21
C(2)–C(7)	1.93	−13.3	0.2	1.94	−14.4	0.14
Zn(1)–O(1)	0.63	11.4	0.06	0.64	12.0	0.03
Zn(1)–N(1)	0.59	8.4	0.07	0.59	8.5	0.08
Zn···H				0.10	0.9	0.71

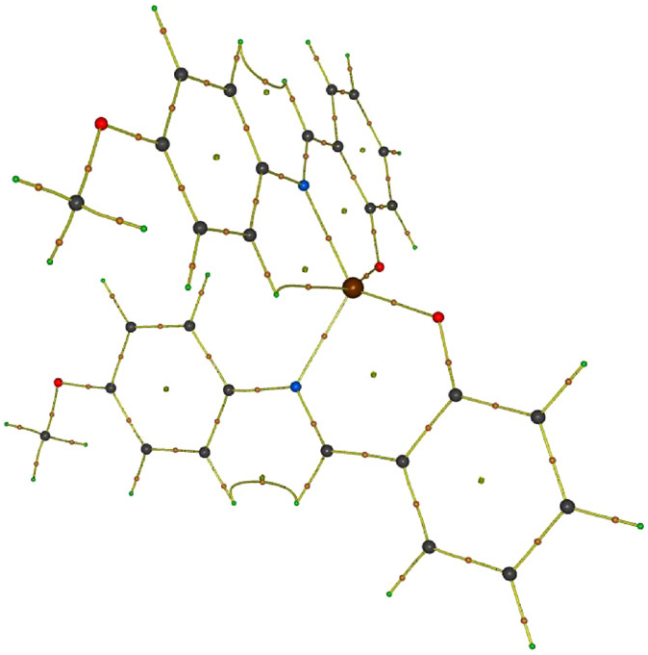

Fig. 6. The molecular graph of $Zn(SH3)_2$ (CPs (3,−1) – pink; (3,+1) – blue and (3,+3) – red). (For interpretation of the references to color in this figure legend, the reader is referred to the web version of the article.)

For both complexes the estimation of coordination bond energy by means of Espinosa's correlation scheme has revealed that the energy for the Zn–O bond (50.2 kcal/mol) is significantly higher than that for the Zn–N one (39.8 kcal/mol). In its turn the Zn···H interaction energy in $Zn(SH3)_2$ complex is equal to 2.6 kcal/mol that is comparable to the values usually observed for C–H···O interactions [44]. It should be noted that this energy value is significantly higher than the ones (∼0.8 kcal/mol) recently observed for intermolecular Pd···H interactions [45,46].

The atomic charge values obtained by integration of $\rho(\mathbf{r})$ within the atomic basins ($\boldsymbol{\Omega}$) surrounded by zero-flux surface are given in Table 4. The accuracy of obtained charges can be partly justified by the values of Lagrangian [$L(\mathbf{r}) = -1/4\nabla^2\rho(\mathbf{r})$] and volumes, obtained by the analogues procedure. In particular, the $L(\mathbf{r})$ value for Zn atoms is smaller than 2.0×10^{-4} a.u. [47] Thus, the sum of the atomic volumes in the crystals $Zn(SH1)_2$ and $Zn(SH3)_2$ (554.07 and 574.00 Å^3) reproduces well the volume of the independent part of the unit cell (550.32(5) and 576.53(4) Å^3), the error being only 0.7 and 0.4%. From Table 4 it is evident that for both molecules the charges of the respective atoms of the chelate cycle as well as of ipso-atom of *para*-substituted phenyl (see Fig. 4) are the same.

Table 4
Selected atomic charges (e) of $Zn(SH1)_2$, $Zn(SH3)_2$ complexes.

Atoms	$Zn(SH1)_2$	$Zn(SH3)_2$
Zn	0.37	0.35
O	−0.83	−0.85
N	−0.97	−0.93
C(1)	0.48	0.52
C(2)	−0.08	−0.11
C(3)	0.34	0.36
C(4)	0.19	0.17

The analysis of CPs in the interatomic area has revealed that molecules participate in a number of weak interactions all of which correspond to the closed-shell ones. Although the majority of them are H···H and C···H ones one can also find bond paths for stacking interaction in $Zn(SH3)_2$. The energy of all contacts estimated above by means of Espinosa's correlation [42] does not exceed 1.0 kcal/mol. As it was recently proposed [44], the sum of all energies for intermolecular contacts should give us the value of sublimation enthalpy of the compound. Using this approach we have obtained the sublimation enthalpy for $Zn(SH1)_2$ and $Zn(SH3)_2$ equal to 15.2 and 17.2 kcal/mol. The slight increase in the lattice energy agrees well with the increase in atomic volume for the latter complex. Moreover, these values are at the same order of magnitude as the ones obtained experimentally using effusion method for similar ZnSalen complex (H_2Salen = *N*,*N*′-bis(salicylaldehydo)ethylenediamine) [48].

Thus, summarizing the results of the X-ray diffraction analysis and the topological analysis of the electron density function we can conclude that the change of the substituent R (Fig. 4) does not affect significantly the bond lengths and charge distribution in the chelate cycles.

3.3. Thermal analysis

One of the most important requirements for a new compound to be used as EL materials is the thermal stability [16(b)]. Information about this stability regarding temperature can be estimated from the weight loss curves obtained from routine thermogravimetric measurements. Usually, the temperature at which the weight loss starts (T_b) is defined as the highest temperature at which the compound is still thermally stable. The analysis of the thermal stability was performed for all Schiff bases and zinc complexes investigated in this work (Fig. 7).

The weight loss curves of HL follows a one step process (Fig. 7(a)), characterized by a total weight loss of 100%. The T_b for Schiff bases lays in the range 100–150 °C. For zinc complexes weight loss occurs in two steps with T_b temperature being around 190 °C. Thus, formation of the complex induces an increase of the thermal stability. The total weight loss for all complexes corresponds to their decomposition into zinc oxide.

3.4. Optical properties

Photoluminescent (PL) properties of the organic molecules can be easily tuned by changing the nature of the substituents or

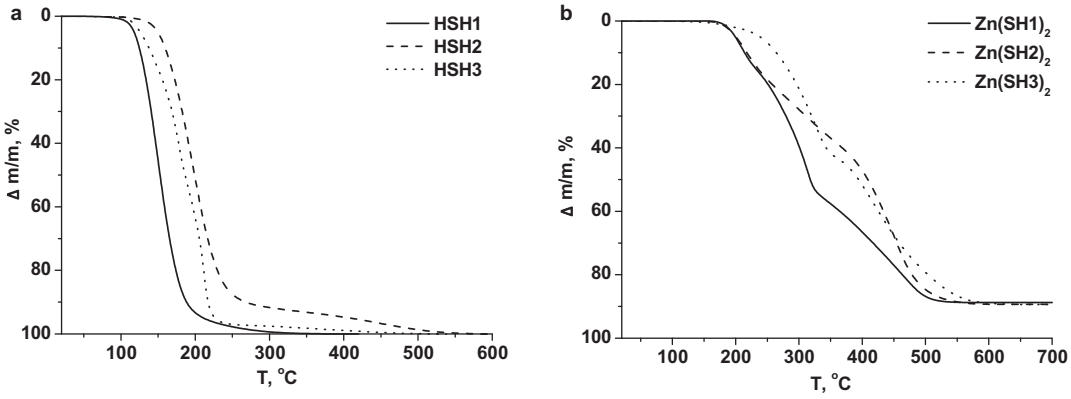

Fig. 7. Curves of weight loss for HL and ZnL_2 under nitrogen atmosphere.

through the complex formation with different metals [49]. The luminescence of zinc complexes usually occurs at energies corresponding to transitions between the electronic levels of organic ligands. Therefore, optical properties of such compounds are very sensitive to the composition and structural parameters of the molecule that is the same as for organic molecules. Herein, an influence of: (1) an introduction of substituents possessing different inductive and/or mesomeric effects and (2) zinc complex formation on the PL properties of bidentate Schiff bases is demonstrated. To follow this three parameters are considered: (1) the position of the maxima in PL spectra, (2) the PL quantum yield, and (3) lifetime of the excited state.

Absorption spectra. The electron transitions possible in HL and ZnL_2 were investigated based on the absorption spectra of the solutions in methanol (Fig. 8). The overall shape of the spectra is very similar. In the case of HL, the absorption bands observed in the 220–300 nm range correspond to the electronic transitions from the amine fragment of the molecule to an azomethine bond while the bands in the 300–500 nm region is attributed to the ones from the aldehyde fragment to the azomethine bond [50,51]. Besides that, based on the analysis of a wide range of absorption spectra of azomethine organic molecules [52], it is reasonable to conclude that the long wavelength bands in the absorption spectra of HL correspond to the formation of the *keto-enamine* isomer in the solution.

Experimental spectroscopic investigations have been supported by TD-DFT theoretical modeling. The equilibrium geometries and frontier molecular orbitals of HL in *enol-imine* and *keto-enamine* form are presented in Tables S6, S7, Supporting Information. The comparison of the experimental absorption (Table S8, Supporting Information) and theoretical bands (Table S9, Supporting Information) shows that the best match between them can be achieved when considering the simultaneous presence of both tautomeric forms in solution, namely the *keto-enamine* and *enol-imine* isomers as well as reveals the nature of the bands. Thus, the equilibrium between the *enol* and *keto* forms (Fig. 1) exists in solution of HL.

As shown in Table S8, the most intense absorption bands of HL occur at 340 nm (HSH1), 383 nm (HSH2) and 348 nm (HSH3). It has been demonstrated that the deprotonation and coordination of Schiff bases to zinc metal ions can significantly reduce the energy gap between HOMOs and LUMOs [53]. TDDFT calculations have been performed on ZnL_2 complexes and shown that the HOMO–LUMO energy separation of the complexes becomes smaller (see Fig. 9, *tautomer* (1) and Fig. 10).

As a result, absorption maxima of zinc complexes are red shifted compared to HL and occur at 385 nm ($Zn(SH1)_2$), 400 nm ($Zn(SH2)_2$), 386 nm ($Zn(SH3)_2$).

Photoluminescent properties. The excitation wavelength was chosen based on the absorption and reflection spectra of the compounds in solution and solid state, respectively (Fig. 8, S2, S3, Supporting Information). All the Schiff bases and zinc complexes possess a PL in the visible spectral range (Fig. 11; Table 5). The PL spectra of all solid state samples with exception for HSH3 at 77 K display more pronounced fine structure and a hypsochromic shift in comparison with the ones at 298 K (Fig. 11(a, b)).

Based on the absorption data of HL and ZnL_2 (Fig. 8; Table S8, Supporting Information) and their theoretical simulation (Tables S9, S10), one can assign the broad emission band observed

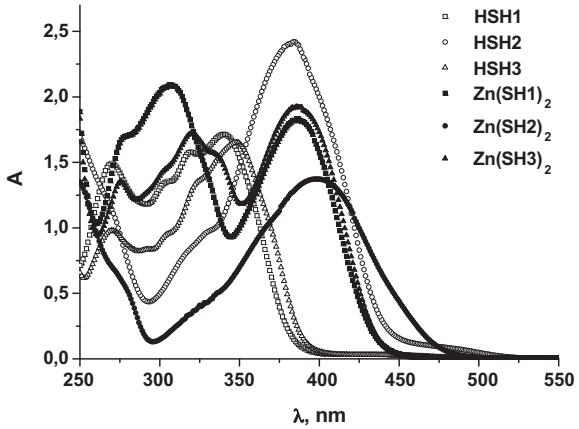

Fig. 8. Absorption spectra of HL, ZnL_2 in methanol, $c = 10^{-5}$ M.

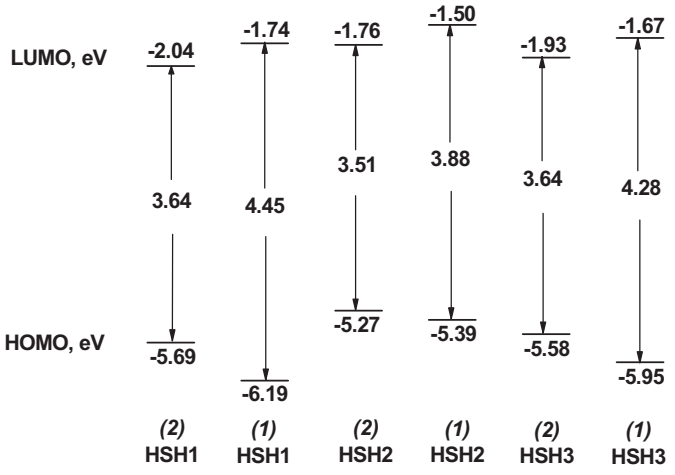

Fig. 9. Schematic representation of energy gap between HOMO and LUMO for (1) *enol-imine* and (2) *keto-enamine* tautomers of HL (DFT/PBE0).

Table 5
Photophysical properties (λ_{ex} = 337 nm) of HL and ZnL_2 measured in solid state; T = 298 K.

Compound	Solid state							
	λ, nm	Q, %[a]	τ_1, ns	τ_2, ns	f_1, %	f_2, %	$k_r \times 10^7$, s^{-1}	$k_{nr} \times 10^7$, s^{-1}
HSH1	552	24.8 ± 0.4	–	–	–	–	–	–
HSH2	612	13.9	–	–	–	–	–	–
HSH3	559	1.0	–	–	–	–	–	–
$Zn(SH1)_2$	521	32.8	0.31	1.91	7.57	92.43	17.18	35.18
$Zn(SH2)_2$	547; 577	27.6	0.17	1.02	14.79	85.21	27.07	70.97
$Zn(SH3)_2$	524	18.0	0.65	1.89	15.09	84.91	9.50	43.41

[a] The quantum yields of HSH2, HSH3 and ZnL_2 were calculated relative to the value of absolute quantum yield of HSH1 (see experimental details).

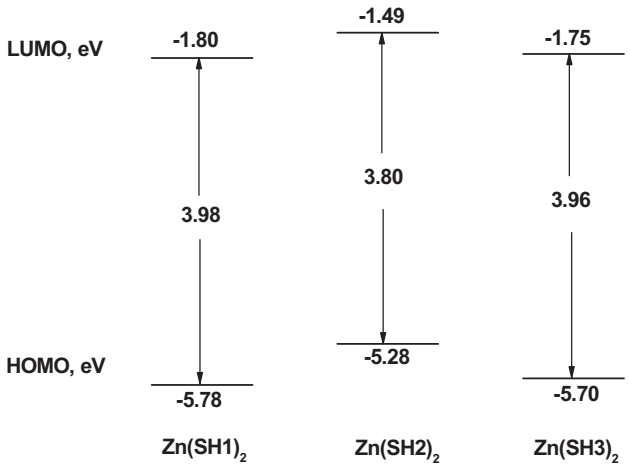

Fig. 10. Schematic representations of energy gap between the HOMO and LUMO for ZnL_2 (DFT/B3LYP).

in the PL spectra of HL (Fig. 11(a)) to the electron transfer from the highest occupied (HOMO) to the lowest unoccupied (LUMO) molecular orbitals. The HOMO of each ligand has a pronounced π-bonding character while the LUMO is primary a π*-antibonding molecular orbital of the Schiff base. Therefore, this broad emission band corresponds to a $\pi \rightarrow \pi^*$ transition. In a similar way, the emission bands observed in the zinc complexes (Fig. 11(b)) can be attributed to a $\pi \rightarrow \pi^*$ electron transfer taking place between the ligand orbitals (ligand-to-ligand charge transfer, LLCT).

Schiff bases. The maxima in PL spectra of HSH2 are red shifted in comparison with the ones for HSH1 (Fig. 11; Table 5). While the molecules of HSH1 and HSH2 are both flat and their crystal packing can be described from the viewpoint of "piles" or "tiles", the substituents are located in the plane of amine fragment [34–36]. Therefore, the extension of the electronic density on the azomethine nitrogen atom (C=N) occurs due to the positive mesomeric effect of $-N(CH_3)_2$ located in the *para*-position of the amine ring (HSH2). This effect results in the enhancement of N···H–O interaction for HSH2 molecules ($d(O1\cdots N1)_{HSH1}$ = 2.602 Å, $d(O1\cdots N1)_{HSH2}$ = 2.564 Å) in comparison with HSH1. Thus, the *keto-enol* equilibrium is noticeably more shifted to the *keto-enamine* tautomeric form in the case of HSH2 compared to that for HSH1. This can be also confirmed by the appearance in the absorption spectrum of HSH2 the band at 400 nm [36]. As a consequence the structure of the molecular orbitals is changed leading to a reduction of the gap between HOMO and LUMO. The details of these findings were previously described in the literature [54,55]. The experiment observations are in good agreement with the results of theoretical calculations (Fig. 9; Table S7, Supporting Information).

The crystal structure of HSH3 (R = $-OCH_3$) is unknown. However, the character of the absorption spectra measured in methanol solution (Fig. 8) for HSH1 and HSH3 are very similar. It means that both systems contain approximately equal quantities of the molecules in quinoid form. In addition, theoretical calculations data shows that values of the energy gap between the HOMO and LUMO for HSH1 and HSH3 are very similar (Fig. 9). Consequently, the energy of the maxima in the PL spectra for these two ligands are almost identical (Fig. 11(a); Table 5).

The quantum yield values for HL in solid state changes in the following order: HSH1 > HSH2 > HSH3 (Table 5). The observed quenching of HSH3 luminescence could be attributed to the presence of the sublevels that could lower the energy gap between singlet and triplet state and thus enhance the intersystem crossing due to peculiarities of molecules orientation. The absolute quantum yield was measured only for HSH1 in the solid state and was equal to 24.8 ± 0.4% (Table 5).

Zinc complexes with Schiff bases. It worth noting that the emission maxima of complexes in the solid state displayed a ~30–40 nm red shift compared to the results of the previous studies performed in dimethylformamide [12]. This can be attributed to the formation of different types of interactions between the molecules in the solid state (for example, π–π* stacking, *etc.*) [56].

According to the energy gap law for radiationless deactivation [57], the luminescence of ZnL_2 should be red shifted compare

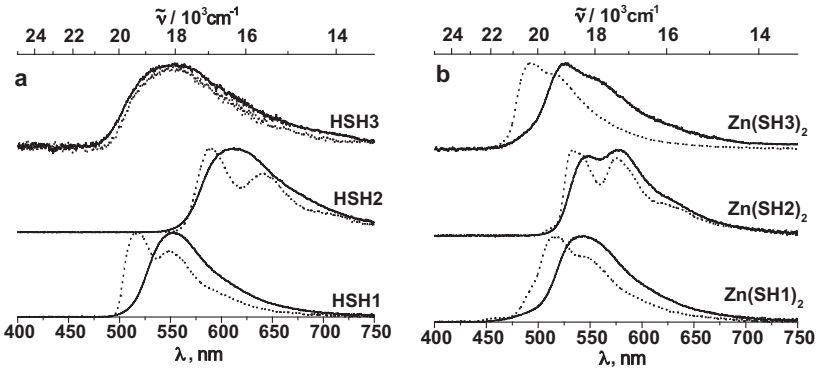

Fig. 11. Luminescence spectra of (a) HL and (b) ZnL_2 in solid state at — 298 K, - - - 77 K.

with their corresponding ligands similar to what was observed in the absorption spectra [53]. However, the analysis of our results shows the reverse trend (Fig. 11; Table 5). The analogous discrepancy in dependences were described in several works [58–60] and explained by excited state intramolecular proton-electron transfer (ESIPT) which is followed by an *enol-keto* tautomerism (Fig. 1). The proton transfer resulted in the formation of low energy tautomeric form and, thus, leaded to: (1) large Stokes shift observed for Schiff bases; (2) a considerable red shift of the luminescent maximum for HL in comparison with ZnL_2 (Table 5). The possibility of the proton transfer was described above based on experimental absorption spectra and theoretical calculations (Figs. 8 and 9). The analysis of the photoluminescent data for the compounds in the solid state shows that the different substituents $-CH_3$, $-N(CH_3)_2$ and $-OCH_3$ have no considerable effect on the position of the emission maximum. These results are consistent with structural data known for these compounds as well as with high resolution X-ray diffraction analysis of electron density distribution performed in this study (see above). The positions of the emission maximum for $Zn(SH1)_2$ and $Zn(SH3)_2$ are almost identical apart from the presence of a more pronounced shoulder at ~570 nm for the latter (Fig. 11(b)). Thus, the replacement of $-CH_3$ by $-OCH_3$ has no strong influence on the energy gap between HOMO and LUMO (Fig. 10) as well as on their localization (Tables S10, S11, S12, Supporting Information) which was supported by theoretical modeling and experimental results [12]. The emission maximum for $Zn(SH2)_2$ is red shifted in comparison with $Zn(SH1)_2$ and $Zn(SH3)_2$. This effect is in agreement with calculated parameters showing the decrease of the energy gap from $Zn(SH1)_2$ to $Zn(SH2)_2$ (Fig. 10). Moreover, the luminescence spectrum of $Zn(SH2)_2$ contains two clearly resolved emission maxima at 547 and 577 nm (Fig. 11(b)). Measurements performed at 77K show a better resolution of the vibronic fine structure of the ZnL_2 emission bands and thus allow determining the value of the vibrational progression for these complexes. This value amounts to $\approx 1360 \pm 100\ cm^{-1}$ and corresponds to a ring breathing mode (see Fig. S4, Supporting Information).

In order to establish the influence of the substituents on the excited state properties of ZnL_2 complexes in the solid state, a series of time-resolved fluorescence experiments were performed. The fluorescence decays were recorded for each sample at four different excitation wavelengths (λ_{ex} = 290, 355, 380, 400 nm), while the detection wavelengths have been selected across the emission spectrum (Table S17, Supporting Information) [61]. The fluorescence decay properties of solid samples ZnL_2 were then globally analyzed and best-fitted as biexponential functions (Table 5, S17, Supporting Information). The lifetime values are similar to these for other zinc complexes with Schiff bases [62]. The analysis of the decay curves fitting shows that pre-exponential factor does not change systematically (Table S17, Supporting Information). Therefore, we can assume the presence of the single emission species. First decay component corresponds to the energy traps caused by the defects in the packing of the molecules. The energy hopping processes in the solid state can enhance the quenching by the presence of these traps in the polycrystalline solid state samples. The decay time [63] of the unquenched molecules can be attributed to τ_2 (see Table 5). For all the complexes the contribution of non-radiative component (k_{nr}) compared to radiative (k_r) one is quite high. The highest influence of this parameter was observed for $Zn(SH3)_2$.

The quantum yields values calculated for zinc complexes are higher than for initial ligands (Table 5). The decrease of relative quantum yields when going from $Zn(SH1)_2$ through $Zn(SH2)_2$ to $Zn(SH3)_2$ can be explained by the appearance of additional states that increase the impact of non-radiative decay processes. For example, in the case of $Zn(SH2)_2$ and $Zn(SH3)_2$ it could be the formation of the additional $\pi\pi^*$ states due to the introduction of $-N(CH_3)_2$ and $-OCH_3$ substituents in the *para*-position of the aniline benzene ring. Moreover, the low quantum yield of $Zn(SH3)_2$ could be related to the possible formation of the additional state because of the presence of the stacking interaction between $SH3^-$ ligands (Fig. S1, Supporting Information) [56] enhancing nonradiative transitions and thus the luminescence quenching compared to the first complexes. Both $Zn(SH1)_2$ and $Zn(SH2)_2$ in the solid state possess relatively high luminescence quantum yields (~20–30%) opening different possibilities for their application as optical materials.

4. Conclusion

In this study we have investigated the influence of the nature of the substituents R = $-CH_3$, $-N(CH_3)_2$, $-OCH_3$ in *para*-position of aniline benzene ring and zinc complexes formation of bidentate *N,O*-donor Schiff bases (HL = HSH1, HSH2, HSH3) on their structural and optical properties. The X-ray diffraction analysis of zinc complexes including topological analysis of electron density reveals that independently on the substituents the main geometrical parameters within the investigated row of the compounds remain almost unchanged. The intermolecular contacts in all zinc complexes correspond to weak van der Waals intermolecular interactions with the only exception of $Zn(SH3)_2$ where the stacking interaction was observed. The analysis of the chemical bonding performed by charge density analysis for $Zn(SH1)_2$ and $Zn(SH3)_2$ allows us to conclude that in $Zn(SH3)_2$ complex the coordination number of zinc atom is five due to the presence of shortened intramolecular Zn···H contact while in both other complexes it is four. Moreover, using topological analysis of electronic density we have obtained the sublimation enthalpy for $Zn(SH1)_2$ and $Zn(SH3)_2$ equal to 15.2 and 17.2 kcal/mol.

Based on the data of absorption spectroscopy and theoretical calculations it is possible to conclude that the broad emission maximum in PL spectra of HL and ZnL_2 are associated with the energy transfer between HOMO and LUMO, corresponding in this case to $\pi \rightarrow \pi^*$ transition. The emission maxima of all the compounds measured in the solid state are red shifted in comparison with these obtained in solution [12] possibly due to the different types of the interaction between the molecules (for example, short contacts, π–π^* stacking, *etc.*) in the solid state. The substitution of $-CH_3$ group by $-OCH_3$ for both HSH1–HSH3 and $Zn(SH1)_2$–$Zn(SH3)_2$ pairs of compounds does not significantly effect the emission maxima while having a slightly larger influence on the vibronic structure of the PL spectra. The maxima in PL spectra of HSH2 and $Zn(SH2)_2$ are red shifted compared to HSH1, HSH3 and $Zn(SH1)_2$, $Zn(SH3)_2$, respectively, due to the strongest mesomeric effect of $-N(CH_3)_2$ group. The latter effect is responsible of the decrease of the energy gap between HOMO and LUMO as well as of the shift of *keto-enol* equilibrium towards the formation of keto-enamine tautomeric form in the case of HSH2 compared to HSH1 and HSH3. Formation of Zn complexes when going from HL to ZnL_2 results not only in the blue shift of emission maxima caused by excited state intermolecular proton-electron transfer in Schiff bases [58–60] but also in a considerable enhancement of luminescence efficiency. Among HL the highest quantum yield equal to $24.8 \pm 0.4\%$ was observed for HSH1. The quantum yield of zinc complexes decreases when going from $Zn(SH1)_2$ to $Zn(SH2)_2$ and $Zn(SH3)_2$ due to the formation of addition levels resulted in nonradiative transitions with the following luminescence quenching with the highest value of ~32.8% for $Zn(SH1)_2$. The fluorescence decays were recorded for ZnL_2 complexes and extracted lifetimes varies from 1.02 up to 1.91 ns (Table 5).

In conclusion, zinc complexes investigated in this work possess adequate optical properties and can be applied not only in OLEDs [12] but also as building blocks for the design of supramolecular polymers [64] for having potential application in surface, separa-

tion and storage science, sensors [5] and as precursors for synthesis of nanosized materials, *etc*. [8].

Acknowledgments

We thank Dr. A.A. Borissenko (Organic Chemistry Division, Lomonosov Moscow State University) for measuring NMR spectra, I.V. Kolesnik (Department of Materials Sciences, Lomonosov Moscow State University) for measuring IR spectra, Dr. T.P. Popova (Center for Drug Chemistry, Moscow) for elemental analysis, Dr. S. Comby and Prof. J.-C. G. Bünzli (Ecole Polytechnique Fédérale de Lausanne, Switzerland) for the determination of absolute quantum yield for HSH1 (solid state sample) and Prof. Peter Burger (Institute of Inorganic and Applied Chemistry, University of Hamburg) for providing an access to computational power. Also we thank the Russian Foundation for Basic Research (grants 05-03-33090-a, 07-02-00495-a, 09-03-00603-a) and Ministry of Education and Science of the Russian Federation (grant RNP 2.1.1/2371) for financial support.

Appendix A. Supplementary data

Supplementary data associated with this article can be found, in the online version, at doi:10.1016/j.jphotochem.2010.12.011.

References

[1] (a) P.A. Vigato, S. Tamburini, The challenge of cyclic and acyclic Schiff bases and related derivatives, Coord. Chem. Rev. 248 (2004) 1717–2128;
(b) K.C. Gupta, A.K. Sutar, C.C. Lin, Polymer supported Schiff base complexes in oxidation reactions, Coord. Chem. Rev. 253 (2009) 1926–1946;
(c) A.D. Garnovskii, I.S. Vasilchenko, D.A. Garnovskii, B.I. Kharisov, Molecular design of mononuclear complexes of acyclic Schiff base ligands, J. Coord. Chem. 62 (2009) 151–204;
(d) R. Hernandez Molina, A. MederoS, Acyclic and macrocyclic Schiff base ligands, in: J.A. McCleverty, T.J. Meyer (Eds.), Comprehensive Coordination Chemistry II, vol. 1, Elsevier, Amsterdam, 2004, pp. 411–474;
(e) S.J. Wezenberg, A.W. Kleij, Material applications for Salen frameworks, Angew. Chem. Int. Ed. 47 (2008) 2354–2364.

[2] (a) B.N. Shelimov, Untraditional methods for activation of oxide catalysts with deposited ions of transition metals, Ross. Khim. Jurn. 44 (2000) 57–70;
(b) K.C. Gupta, A.K. Sutar, Catalytic activities of Schiff base transition metal complexes, Coord. Chem. Rev. 252 (2008) 1420–1450;
(c) T. Katsuki, Unique asymmetric catalysis of *cis*-β metal complexes of salen and its related Schiff-base ligand, Chem. Soc. Rev. 33 (2004) 437–444;
(d) P.G. Gozzi, Metal-Salen Schiff base complexes in catalysis: practical aspects, Chem. Soc. Rev. 33 (2004) 410–421;
(e) F. Blank, C. Janiak, Metal catalyst for the vinyl/addition polymerization of norborene, Coord. Chem. Rev. 253 (2009) 827–861.

[3] (a) B. Weber, Spin crossover complexes with N_4O_2 coordination sphere—the influence of covalent linkers on cooperative interactions, Coord. Chem. Rev. 253 (2009) 2432–2449;
(b) A.D. Garnovskii, V.N. Ikorskii, A.I. Uraev, I.S. Vasilchenko, A.S. Burlov, D.A. Garnovskii, K.A. Lyssenko, V.G. Vlasenko, T.E. Shestakova, Yu.V. Koschienko, T.A. Kuz'manko, L.N. Divaeva, M.P. Bubnov, V.P. Rybalkin, O.Yu. Korshunov, I.V. Pirog, G.S. Borodkin, V.A. Bren, I.E. Uflyand, V.I. Minkin, The novel azomethine ligands for binuclear copper(II) complexes with ferro- and antiferromagnetic properties, J. Coord. Chem. 60 (2007) 1493–1511.

[4] (a) A. Garoufis, S.K. Hadjikakou, N. Hadjiliadis, Palladium coordination compounds as anti-viral, anti-fungal, anti-microbial and anti-tumor agents, Coord. Chem. Rev. 253 (2009) 1384–1397;
(b) H.Q. Chen, S. Hall, B. Zheng, J. Rhodes, Potentiation of the immune system by Schiff-base forming drugs: mechanism of action and therapeutic potential, Biodrugs 7 (1997) 217–231.

[5] (a) C. Lordeiro, F. Pina, Luminescent and chromogenic molecular probes based on polyamides and related compounds, Coord. Chem. Rev. 253 (2009) 1353–1383;
(b) S. Khatua, S.H. Chol, J. Lee, J.O. Huh, Y. Do, D.G. Churchlll, Highly selective fluorescence detection of Cu^{2+} in water by chiral dimeric Zn^{2+} complexes through direct displacement, Inorg. Chem. 48 (2009) 1799–1801;
(c) M. Cano, L. Rodríguez, J.C. Lima, F. Pina, A.D. Cort, C. Pasquini, L. Schiaffino, Specific supramolecular interactions between Zn^{2+}-Salophen complexes and biologically relevant anions, Inorg. Chem. 48 (2009) 6229–6235.

[6] (a) P.G. Cozzi, L.S. Dolci, A. Garelli, M. Montalti, L. Prodi, N. Zaccheroni, Photophysical properties of Schiff-base metal complexes, New J. Chem. 27 (2003) 692–697;
(b) A.V. Metelitsa, A.S. Burlov, S.O. Bezuglii, I.G. Borodkina, V.A. Bren, A.D. Garnovskii, V.I. Minkin, Luminescent complexes with ligands containing C=N bond, Russ. J. Coord. Chem. 32 (2006) 858–868.

[7] (a) Q. Hou, L. Zhao, H. Zhang, Y. Wang, S. Jiang, Synthesis and luminescent properties of two Schiff-base boron complexes, J. Luminesc. 126 (2007) 447–451;
(b) K.Y. Hwang, M.H. Lee, H. Jang, Y. Sung, J.S. Lee, S.H. Kim, Y. Do, Aluminium-salen luminophores as new hole-blocking materials for phosphorescent OLEDs, Dalton Trans. 14 (2008) 1818–1820.

[8] (a) S. Jung, W. Cho, H.J. Lee, M. Oh, Self-template-directed formation of coordination-polymer hexagonal tubes and rings, and their calcination to ZnO rings, Angew. Chem. Int. Ed. 48 (2009) 1459–1462;
(b) T. Kaczorowski, I. Justyniak, T. Lipinska, J. Lipkowski, J. Lewinski, Metal complexes of cinchonine as chiral building blocks: a strategy for the construction of nanotubular architectures and helical coordination polymers, J. Am. Chem. Soc. 131 (2009) 5393–5395.

[9] H.C.S. Kumar, B.R. Bhat, B.J. Rudresha, R. Ravindra, R. Philip, Synthesis, characterisation of *N*,*N*′-bis(2-hydroxynaphthalidene)phenylene-1,2-diamine with M(II) (M = Ni, Zn and Fe) Schiff base complexes and their non-linear optical studies by z-scan technique, Chem. Phys. Lett. 494 (2010) 95–99.

[10] (a) M.E. Germain, T.R. Vargo, P.G. Khalifah, M.J. Knapp, Fluorescent detection of nitroaromatics and 2,3-dimethyl-2,3-dinitrobutane (DMNB) by zinc complex: (salophen)Zn, Inorg. Chem. 46 (2007) 4422–4429;
(b) M.E. Germain, M.J. Knapp, Discrimination of nitroaromatics and explosives mimics by a fluorescent Zn(salicylaldimine) sensor array, J. Am. Chem. Soc. 130 (2008) 5422–5423;
(c) S. Khatua, S.H. Choi, J. Lee, K. Kim, Y. Do, Aqueous fluorometric and colorimetric sensing of phosphate ions by a fluorescent dinuclear zinc complexes, Inorg. Chem. 48 (2009) 2993–2999.

[11] (a) M.D. Deda, M. Ghedini, I. Aiello, A. Grisolia, A new blue photoluminescent Salen-like zinc complex with excellent emission quantum yield, Chem. Lett. 33 (2004) 1060–1061;
(b) M.G. Kaplunov, S.S. Krasnikova, I.K. Yakushchenko, S.N. Shamaev, A.P. Pivovarov, O.N. Efimov, New organic electroluminescent materials, Mol. Cryst. Liq. Cryst. 426 (2005) 287–293;
(c) T. Yu, W. Su, W. Li, Z. Hong, R. Hua, M. Li, B. Chu, B. Li, Z. Zhang, Z.Z. Hu, Synthesis, crystal structure and electroluminescent properties of a Schiff base zinc complex, Inorg. Chim. Acta 359 (2006) 2246–2251.

[12] (a) J. Xie, J. Qiao, L. Wang, J. Xie, Y. Qiu, An azomethin-zinc complex for organic electroluminescence: crystal structure, thermal stability and optoelectronic properties, Inorg. Chim. Acta 358 (2005) 4451–4458;
(b) L. Chen, J. Qiao, J. Xie, L. Duan, D. Zhang, Substituted azomethine-zinc complexes: thermal stability, electrochemical and electron transport properties, Inorg. Chim. Acta 362 (2009) 2327–2333.

[13] (a) S. Eliseeva, O. Kotova, O. Mirzov, K. Anikin, L. Lepnev, E. Perevedentseva, A. Vitukhnovsky, N. Kuzmina, Electroluminescent properties of the mixed-ligand complex of terbium salicylate with triphenylphosphine oxide, Synth. Met. 141 (2004) 225–230;
(b) O.V. Kotova, S.V. Eliseeva, E.V. Perevedentseva, T.F. Limonova, R.A. Baigeldieva, A.G. Vitukhnovsky, N.P. Kuzmina, The topography of organic light-emitting diode-component functional layers as studied by atomic force microscopy, Mendeleev Commun. (2004) 155–157;
(c) L. Lepnev, A. Vaschenko, A. Vitukhnovsky, S. Eliseeva, O. Kotova, S. Torgova, N. Kuzmina, Two-diode organic light amplifiers/converters and percularities of photocurrent multiplication, Synth. Met. 156 (2006) 624–632;
(d) O.V. Kotova, S.V. Eliseeva, A.A. Volosnikov, V.A. Oleinikov, L.S. Lepnev, A.G. Vitukhnovsky, N.P. Kuzmina, Influence of heteroligand complexation on the thermal, photoluminescent, and film forming properties of some aromatic terbium(III) carboxylates, Russ. J. Coord. Chem. 32 (2006) 901–909;
(e) O.V. Kotova, V.V. Utochnikova, S.V. Eliseeva, S.V. Samoilenkov, N.P. Kuzmina, Gas-phase synthesis of lanthanide(III) benzoates $Ln(Bz)_3$ (Ln = La, Tb, Lu), Russ. J. Coord. Chem. 33 (2007) 454–457.

[14] (a) A.S. Burlov, D.A. Garnovskii, L.I. Kuznetsova, N.V. Volbushko, O.Yu. Korshunov, O.T. Asmaev, B.I. Kharisov, L.M. Blanco, A.D. Garnovskii, Tridentate *o*-tosylaminoazomethines and their complexes with zinc and cadmium: synthesis and spectral-luminescent properties, Russ. J. Coord. Chem. 24 (1998) 857–860;
(b) M.G. Kaplunov, I.R. Yakushchenko, S.S. Krasnikova, S.N. Shamaev, A.P. Pivovarov, O.N. Efimov, New electroluminescent materials based on chelate zinc complexes, Russ. Chem. Bull. 53 (2004) 2148–2151.

[15] (a) O.V. Kotova, S.V. Eliseeva, A.S. Averjushkin, L.S. Lepnev, A.A. Vaschenko, A.Yu. Rogachev, A.G. Vitukhnovsky, N.P. Kuzmina, Zinc(II) complexes with Schiff bases derived from ethylenediamine and salicylaldehyde: the synthesis and photoluminescent properties, Russ. Chem. Bull. Intern. Ed. 57 (2008) 1880–1889;
(b) L. Lepnev, A. Vaschenko, A. Vitukhnovsky, S. Eliseeva, O. Kotova, N. Kuzmina, OLEDs based on some mixed-ligand terbium carboxylates and zinc complexes with tetradentate Schiff bases: mechanisms of electroluminescent degradation, Synth. Met. 159 (2009) 625–631;
(c) O. Kotova, S. Semenov, S. Eliseeva, S. Troyanov, K. Lyssenko, N. Kuzmina, New helical zinc complexes with Schiff base derivatives of β-diketonates or β-keto esters and ethylenediamine, Eur. J. Inorg. Chem. (2009) 3467–3474.

[16] (a) C.H. Chen, J. Shi, Metal chelates as emitting materials for organic electroluminescence, Coord. Chem. Rev. 171 (1998) 161–174;
(b) S. Wang, Luminescence and electroluminescence of Al(III), B(III), Be(II) and Zn(II) complexes with nitrogen donors, Coord. Chem. Rev. 215 (2001) 79–98;

(c) J. Kido, Y. Okamoto, Organo lanthanide complexes for electroluminescent materials, Chem. Rev. 102 (2002) 2357–2368.
[17] SADABS, version 2004/1; Bruker AXS Inc., Madison, WI. XPREP, version 2005/2; Bruker AXS Inc., Madison, WI.
[18] SHELXTL, version 6.1, Bruker AXS Inc., Madison, WI, 2005.
[19] N.K. Hansen, P. Coppens, Testing aspherical atom refinements on small molecule data sets, Acta Crystallogr. A 34 (1978) 909–921.
[20] A. Volkov, P. Macchi, L.J. Farrugia, C. Gatti, P. Mallinson, T. Richter, T. Koritsanszky, XD2006, SUNY at Buffalo, Buffalo, NY, 2006.
[21] F.L. Hirshfeld, Can X-ray data distinguish bonding effects from vibrational smearing? Acta Crystallogr. A 32 (1976) 239–244.
[22] R.F.W. Bader, Atoms in Molecules. A Quantum Theory, Clarendon Press, Oxford, 1990.
[23] A. Stash, V. Tsirelson, WinXPRO: a program for calculating crystal and molecular properties using multipole parameters of the electron density, J. Appl. Cryst. 35 (2002) 371–373.
[24] (a) G.A. Crosby, J.N. Demas, Measurements of photoluminescence quantum yields, Review 75 (1971) 991–1024;
(b) F. Gumy, Patent application PCT/IB 2007/054187 (2007).
[25] (a) A. Bril, A.W. de Jager-Veenis, Quantum efficiency standard for ultraviolet and visible excitation, J. Electrochem. Soc. 123 (1976) 396–398;
(b) A. Bril, Luminescence of Organic and Inorganic Materials, Wiley, Eindhoven, 1962, p. 479.
[26] A.A. Granovsky, PC GAMESS/Firefly (version 7.1.C), http://classic.chem.msu.ru/gran/gamess/index.html.
[27] ChemCraft (version 1.6), www.chemcraftprog.com.
[28] (a) J.P. Perdew, K. Burke, M. Ernzerhof, Generalized gradient approximation made simple, Phys. Rev. Lett. 77 (1996) 3865–3868;
(b) J.P. Perdew, K. Burke, M. ErnzerhoF, Generalized gradient approximation made simple, Phys. Rev. Lett. 78 (1997) 1396–11396.
[29] (a) C. Lee, W. Yang, R.G. Parr, Development of the Colle-Salvetti correlation-energy formula into a functional of the electron density, Phys. Rev. B: Condens. Matter 37 (1988) 785–789;
(b) S.H. Vosko, L. Wilk, M. Nusair, Accurate spin-dependent electron liquid correlation energies for local spin density calculations: a critical analysis, Can. J. Phys. 58 (1980) 1200–1211;
(c) A.D. Becke, Density-functional thermochemistry. III. The role of exact exchange, J. Chem. Phys. 98 (1993) 5648–5652.
[30] E.J. Baerends, O.V. Gritsenko, R. van Leeuwen (Eds.), Chemical Applications of Density Functional Theory; ACS Symposium Series No. 269: Am. Chem. Soc., vol. 20, 1996, pp. 20–35.
[31] R. Stowasser, R. Hoffmann, What do the Kohn-Sham orbitals and eigenvalues mean? J. Am. Chem. Soc. 121 (1999) 3414–3420.
[32] M. Rodríguez, R. Santillan, L. López, N. Farfán, V. Barba, K. Nakatani, E.V. García Baèz, I.I. Padilla-Martínez, N–H···O assisted structural changes induced on ketoenamine systems, Supramol. Chem. 19 (2007) 641–653.
[33] P. Gilli, V. Bertolasi, V. Frretti, G. Gilli, Evidence for intramolecular N–H···O resonance-assisted hydrogen bonding in β-enaminones and related heterodienes. A combined crystal-structural, IR and NMR spectroscopic, and quantum-mechanical investigation, J. Am. Chem. Soc. 122 (2000) 10405–10417.
[34] O.S. Filipenko, V.I. Ponomarev, B.M. Bolotin, L.O. Atovmyan, Crystal and molecular structure of a red modification of N-salicylidiene-p-dimethylaminoaniline. Planar molecular conformation, Kristallografiya 28 (1983) 889–895.
[35] S.M. Aldoshin, L.O. Atovmyan, V.I. Ponomarev, Structure, spectral-luminescent and thermochromic properties of "yellow" N-salicylidene-p-dimethylaminoaniline crystals, Khimicheskaya fizika 3 (1984) 787–791.
[36] S.M Aldoshin, M.I. Knyazhansky, Ya.R. Timyansky, L.O. Atovmyan, O.A. D'yachenko, Effect of intermolecular interactions on photo- and thermochromic properties of crystalline salicylaldehyde arylimines, Khimicheskaya fizika 8 (1982) 1015–1023.
[37] T. Sogo, J. Romero, A. Sousa, A. De Blas, M.L. Duran, E.E. Castellano, The electrochemical synthesis of neutral zinc(II) complexes of Schiff base ligands. The crystal structure of bis[N-(4-methylphenyl)salicylaldiminato]zinc(II), Z. Naturforsch. Teil B-A. J. Chem. Sci. 43 (1988) 611–625.
[38] L. Xiaolan, C. Hongli, M. Fangming, Chin. J. Org. Chem. 12 (1992) 526.
[39] L. Tatar, D. Ülkü, O. Atakol, Zinc(II) complexes of bidentate Schiff base ligands containing methoxyphenyl and nitrophenyl groups, Acta Crystallogr. C55 (1999) 508–510.
[40] (a) T.S. Koritsanszky, P. CoppenS, Chemical applications of X-ray charge-density analysis, Chem. Rev. 101 (2001) 1583–1628;
(b) C. Gatti, Chemical bonding in crystals: new directions, Z. Kristallogr. 220 (2005) 399–457;
(c) V.G. Tsirelson, R.P. Ozerov, Electron Density and Bonding in Crystals: Principles, Theory and X-ray Diffraction Experiments in Solid State Physics and Chemistry, IOP Publishing Ltd., 1996.;
(d) C. Matta, R.J. Boyd (Eds.), The Quantum Theory of Atoms in Molecules, Wiley-VCH, Weinheim, 2007.
[41] (a) K.A. Lyssenko, Yu.V. Nelyubina, R.G. Kostyanovsky, M.Yu. Antipin, Water clusters in crystal: beyond the "hydrogen-bonding graphs", Chem. Phys. Chem. 7 (2006) 2453–2455;
(b) Yu.V. Nelyubina, I.V. Glukhov, M.Yu. Antipin, K.A. Lyssenko, Higher density does not mean higher stability mystery of paracetamol finally unraveled, Chem. Commun. 46 (2010) 3469–3471.
[42] (a) E. Espinosa, E. MolinS, C. Lecomte, Hydrogen bond strength revealed by topological analysis of experimentally observed electronic densities, Chem. Phys. Lett. 285 (1998) 170–173;
(b) E. Espinosa, I. Alkorta, I. RozaS, J. Elguero, E. MolinS, About the evaluation of the local kinetic, potential and total energy densities in closed-shell interactions, Chem. Phys. Lett. 336 (2001) 457–461.
[43] (a) E.A. Pidko, RA. van Santen, The conformations with alkanes adsorbed on zeolitic cations, Chem. Phys. Chem. 7 (2006) 1657–1660;
(b) L.N. Puntus, K.A. Lyssenko, M.Yu. Antipin, J.-C.G. Bünzli, Role of inner- and outer-sphere bonding in the sensitization of Eu^{III}-luminescence deciphered by combined analysis of experimental electron density distribution function and photophysical data, Inorg. Chem. 47 (2008) 11095–11107;
(c) A.O. Borissova, A.A. Korlyukov, M.Yu. Antipin, K.A. Lyssenko, Estimation of dissociation energy in donor–acceptor complex AuCl·PPh_3 via topological analysis of the experimental electron density distribution function, J. Phys. Chem. A 112 (2008) 11519–11522;
(d) Yu.V. Nelyubina, M.Yu. Antipin, K.A. Lyssenko, Hydrogen bonds between zwitterions: intermediate between classical and charge assisted ones. A case study, J. Phys. Chem. A 113 (2009) 3615–3620;
(e) L.N. Puntus, K.A. Lyssenko, I.S. Pekareva, J.-C.G. Bünzli, Intermolecular interactions as actors in energy transfer processes in lanthanide complexes with 2,2′-bipyridine, J. Phys. Chem. B 113 (2009) 9265–9277.
[44] C.F. Matta, J. Hernández-Trujillo, T.-H. Tang, R.F.W. Bader, Hydrogen–hydrogen bonding: a stabilizing interaction in the molecules and crystals, Chem. Eur. J. 9 (2003) 1940–1951 (and ref. therein).
[45] T.A. Peganova, A.V. Valyaeva, A.M. Kalsin, P.V. Petrovskii, A.O. Borissova, K.A. Lyssenko, N.A. Ustynyuk, Synthesis of aminoiminophosphoranate complexes of palladium and platinum and X-ray diffractional investigation of the weak C–H···Pd interactions affecting the geometry of the PdNPN metallacycles, Organometallics 28 (2009) 3021–3028.
[46] A.O. Borissova, M.Yu. Antipin, D.S. Perekalin, K.A. Lyssenko, Crucial role of Ru···H interactions in the crystal packing of ruthenocene and its derivatives, Cryst. Eng. Comm. 10 (2008) 827–832.
[47] A.M. Grana, R.A. Mosquera, The transferability of the carbonyl group in aldehydes and ketones, J. Chem. Phys. 110 (1999) 6606–6616.
[48] M.D.M.C. Ribeiro da Silva, J.M. Gonçalves, A.L.R. Silva, P.C.F.C. Oliveira, B. Schröder, M.A.V. Ribeiro da Silva, Molecular thermochemical study of Ni(II), Cu(II) and Zn(II) complexes with N,N′-bis(salicylaldehydo)ethylenediamine, J. Mol. Catal. A: Chem. 224 (2004) 207–212.
[49] B. Valeur, Molecular Fluorescence Principles and Applications, Wiley-VCH Verlag CmbH, 2001, p. 381.
[50] Y.P. Kitaev, V.I. Savin, V.V. Zverev, G.V. Popova, Structure and reactivity of nitrogen-containing derivatives of carbonyl compounds. XXXIII. Ultraviolet spectra and structure of 4-(benzylideneamino)-1,2,4-triazole molecules, Khimiya geterotsiklicheskikh soedinenii 4 (1971) 559–564.
[51] M.I. Knyazhanskii, V.S. Orekhovsii, P.V. Gilyarovskii, A.S. Burlov, Fluorescence of N-triazolyl derivatives of azomethines, Khimiya geterotsiklicheskikh soedinenii 4 (1984) 554–556.
[52] M.D. Cohen, G.M.J. Schmidt, Photochromy and thermochromy of anils, J. Phys. Chem. 66 (1962) 2442–2446.
[53] S.-L. Zheng, J.-P. Zhang, X.-M. Chen, Z.-L. Huang, Z.-Y. Lin, W.-T. Wong, Syntheses, structures, photoluminescence, and theoretical studies of a novel class of d^{10} metal complexes of 1*H*-[1,10]phenanthrolin-2-one, Chem. Eur. J. 9 (2003) 3888–3896.
[54] D. LeGourriérec, V.A. Kharlanov, R.G. Brown, W. Rettig, Excited-state intramolecular proton transpher (ESIPT) in 2-(2′-hydroxyphenyl)-oxazole and -thiazole, J. Photochem. Photobiol. A: Chem. 130 (2000) 101–111.
[55] A. Filarowski, Intramolecular hydrogen bonding in o-hydroxyaryl Schiff bases, J. Phys. Org. Chem. 18 (2005) 686–698.
[56] (a) M.E. Germain, T.R. Vargo, P.G. Khalifah, M.J. Knapp, Fluorescent detection of nitroaromatics and 2,3-dimethyl-2,3-dinitrobutane (DMNB) by zinc complex: (salophen)Zn, Inorg. Chem. 46 (2007) 4422–4429;
(b) S. Mizujami, H. Houjou, K. Sugaya, E. Koyama, H. Tokuhisa, T. Sasaki, M. Kanesato, Fluorescence colour modulation by intramolecular and intermolecular π–π interactions in a helical zinc(II) complex, Chem. Mater. 17 (2005) 50–56.
[57] N.J. Turro, Modern Molecular Photochemistry, University Science Books, Sausalito, CA, 1991, p. 628.
[58] Y.-P. Tong, S.-L. Zheng, X.-M. Chen, Structures, photoluminescence and theoretical studies of two Zn^{II} complexes with substituted 2-(2-hydroxyphenyl)benzimidazoles, Eur. J. Inorg. Chem. 18 (2005) 3734–3741.
[59] (a) Y.-P. Tong, S.-L. Zheng, X.-M. Chen, Synthesis, structure, photoluminescence and theoretical studies of a class of beryllium(II) compounds of aromatic *N,O*-chelate ligands, Inorg. Chem. 44 (2005) 4270–4275;
(b) H. Görner, S. Khanra, T. Weyhermüller, P. Chaudhuri, Photoinduced intramolecular proton transpher of phenol-containing ligands and their zinc complexes, J. Phys. Chem. A 110 (2006) 2587–2594.
[60] A.O. Eseola, W. Li, R. Gao, M. Zhang, X. Hao, T. Liang, N.O. Obi-Egbedi, W.-H. Sun, Synthesis, structure, and fluorescent properties of 2-(1H-imidazol-2-yl)phenols and their neutral Zn(II) complexes, Inorg. Chem. 48 (2009) 9133–9146.
[61] N. Boens, W.W. Qin, N. Basaric, J. Hofkens, M. Ameloot, J. Pouget, J.P. Lefevre, B. Valeur, E. Gratton, M. Vandeven, N.D. Silva, Y. Engelborghs, K. Willaert, A. Sillen, G. Rumbles, D. Phillips, A. Visser, A. van Hoek, J.R. Lakowicz, H. Malak, I. Gryczynski, A.G. Szabo, D.T. Krajcarski, N. Tamai, A. Miura, Fluorescence life-

time standards for time and frequency domain fluorescence spectroscopy, Anal. Chem. 79 (2007) 2137–2149.
[62] (a) P. Roy, K. Dhara, M. Manassero, P. Banerjee, Synthesis, characterization and fluorescent zinc(II) sensing property of three Schiff-base compounds, Inorg. Chim. Acta 362 (2009) 2927–2932;
(b) P. Roy, M. Manassero, K. Dhara, P. Banerjee, Synthesis, characterization and fluorescence properties of hexanuclear zinc(II) complexes, Polyhedron 28 (2009) 1133–1137.
[63] J.R Lakowicz, Principles of Fluorescence Spectroscopy, Springer, New York, 2006, p. 954.
[64] (a) J.B. Beck, S.J. Rowan, Multistimuli, multiresponsive metallo-supramolecular polymers, J. Am. Chem. Soc. 125 (2003) 13922–13923;
(b) W. Weng, Z. Li, A.M. Jamienson, S.J. Rowan, Control of gel morphology and properties of a class of metallo-supramolecular polymers by good/poor solvent environments, Macromolecules 42 (2009) 236–246.